Anisotropic correlations of plasticity on the yielding of metallic glasses

Shiheng Cui, Huashan Liu, and Hailong Peng*

School of Materials Science and Engineering, Central South University, 932 South Lushan Road, Changsha 410083, China

(Received 11 January 2022; accepted 7 July 2022; published 21 July 2022)

We report computer simulations on the shear deformation of CuZr metallic glasses at zero and room temperatures. Shear bands emerge in athermal alloys at strain γ_c, with a finite-size effect found. The correlation of nonaffine displacement exhibits an exponential decay even after yielding in thermal alloys, but transits to a power law at $\gamma > \gamma_c$ in athermal ones. The algebraic exponent is around -1 for the decay inside shear bands, consistent with the theoretical prediction in random elastic media. We quantify the anisotropic correlation with harmonic projection, finding the spectrum is weak in the exponential-decay regime, while it displays a strong polar and quadrupolar symmetry in the power-law regime. The nonvanishing quadrupolar symmetry at long distance signifies the nonlocality of plastic correlation in the athermal alloys. In contrast, the plastic correlation was found to be isotropic and localized at the yielding in the thermal alloys without shear bands.

DOI: 10.1103/PhysRevE.106.014607

I. INTRODUCTION

Metallic glasses (MGs) are kinds of amorphous solids of noticeable engineering application due to their unique mechanical properties, e.g., relatively high strength, good elastic deformability, and hardness, compared to the crystalline counterparts [1–3]. The disordered nature of the atomic-level structure renders the response of the amorphous solids inhomogeneous even at the zero-load limit. A nonaffine displacement field exhibits a pattern of vortexlike shape, with the length scale typically about 30 atomic diameters in a two-dimensional system [4,5]. The nonaffine vortex is found to correlate with the breakdown of the elastic continuum limit and is responsible for the boson peak in amorphous solids [6].

Beyond the near harmonic approximation, plastic events represented as atoms moving beyond the original local energy minimum organize in a space of typical features. Upon deformation, the local energy landscape will be changed by external force, with the local energy minimum destabilized and new saddle points emerged [7]. The motion of atoms is, then, dominated by sequential jumps over a series of inherent structures if the thermally activated motion can be neglected. The principle for the organization of the sequential jumps is unclear, but the elastic continuum mechanism recovers, in the sense that the local plastic events can be considered as Eshelby inclusions that cause an anisotropic field in the surrounding matrix [8]. The predicted quadrupolelike anisotropy for stress or strain has been verified in sheared Lennard-Jones solids [9], colloidal systems [10], granular materials [11], and even supercooled liquids [12–14]. The oriented stress field can trigger the birth of a new irreversible flip nearby [9]. A consequence of the interaction leads to the spatial organization of plastic events. This renders the possibility to calculate the size of local irreversible arrangements or the so-called shear-transformation zones in amorphous solids [15–18].

However, it results in a debate for the decay formula of the nonaffine displacement correlation: an exponential decay with a characteristic length scale [18,19] or a power-law decay with nonvanishing long-range correlation [10,20]. There is evidence that a small system size can truncate the power-law decay in large systems into a spurious exponential decay [21]. Besides the finite-size effect, correlation anisotropy is another important ingredient to be considered in the correlation decay, as the plastic events could align in peculiar directions complying with the aforementioned quadrupolelike stress field. For this, a fourfold angular symmetry has been reported for nonaffine displacement correlation in the sheared two-dimensional (2D) Lennard-Jones solids [22,23]. Yet the correlation anisotropy can, on the other hand, be blurred by the thermal fluctuation, as unveiled in hard-sphere colloidal glasses [24].

While most of the works focus on the steady-state flow regime, plastic correlation on the yielding of the metallic glasses is still not well clarified, especially in the samples of distinct mechanical behaviors. In this work, we performed classical molecular dynamics (MD) simulations on CuZr MGs with shear deformation in two different situations: one is the zero-temperature limit where a shear band emerges in all the system sizes that we investigated; the other one is the room temperature where no or weak shear banding is observed. The organization of the plastic events is expected to be different; the athermal system would develop strongly heterogeneous plastic regions as the subextensive scaling unveiled in 2D Lennard-Jones solids [25], while this feature is not detected in thermal systems. Here, we focus on the decaying formula of the plastic correlations, and the quantitative characterization of the anisotropy by projecting the azimuthal-dependent correlator on harmonic spherical functions in these two kinds of MGs that have discrepant mechanical properties.

*hailong.peng@csu.edu.cn

II. SIMULATION DETAILS

Classical MD simulations were conducted for $Cu_{50}Zr_{50}$ alloys with the atomic interaction potential formulated by the embedded-atom method, with the force-field parameters adequate for describing the amorphous state of Cu-Zr metallic glasses [26,27]. Samples of the random configuration were created at $T = 2000$ K, then quenched to 300 K or zero temperature with a cooling rate about 4×10^{11} K/s, during which the NPT ensemble was utilized to adjust the box size to give zero pressure. More details about the sample fabrication can be found in Ref. [28].

Uniform shear deformation was performed via the athermal quasistatic shear (AQS) protocol [29] for alloys at zero temperature. Particle position was affinely transformed: $r_x' = r_x + \Delta\gamma r_y$, with $\Delta\gamma = 2 \times 10^{-4}$ the strain increment in every step. A subsequent potential energy minimization was followed to relax the system to the nearest energy minimum. This procedure is repeated until the largest strain is achieved. For alloys at room temperature (RT, $T = 300$ K), shear deformation was accomplished by the affine transformation of coordinates in every time step in a shear rate of about 2×10^7 s^{-1}, coupled with the Nose-Hoover thermostat. The set of thermostat parameters roughly relaxes the system to the target temperature in a time span of 0.1 ps. To check the effect of the thermostat protocol, we performed independent shear deformation at RT using a Langevin thermostat, with the friction parameter set to 1 ps, a typical relaxation time in liquids. The results from these two methods are consistent in terms of the anisotropic decay and the correlation length obtained. The simulations were carried out with the software package LAMMPS [30]. To check the finite-size effect, four cubic systems are considered: $N = 4 \times 10^4$, $L = 88.7$ Å (with N the number of particles and L the box length); $N = 3.2 \times 10^5$, $L = 177$ Å; $N = 1.1 \times 10^6$, $L = 266$ Å; and $N = 1.1 \times 10^7$, $L = 576$ Å. To improve the statistics, six independent realizations are averaged for the calculation of the correlation functions.

Nonaffine displacement of atoms was evaluated as the deviation of the actual displacement of the nearest neighbors about the central ones to the affine transforming that minimizes the square of the deviation vectors in a strain interval, $\Delta\gamma$ [31,32]:

$$D_i^2(\gamma) = \frac{1}{M}\sum_j [r_{ij}(\gamma) - (\epsilon + \delta_{ij})r_{ij}(\gamma - \Delta\gamma)]^2, \qquad (1)$$

where γ is the strain, ϵ is the strain tensor that gives the minimum nonaffine displacement, and r_{ij} is the vector from atom i to atom j, with j the nearest neighbor of i defined as their distance that is smaller than the first minimum position in the pair distribution function. Note that the nonaffine displacement is normalized by the number of nearest neighbors M, which is different from the original definition [31]. The coordination number of particles depends on their species, e.g., Cu atoms typically have 12 nearest neighbors, while Zr atoms have 16 neighbors. They should not significantly differ in the nonaffine displacement due to the atomic species if embedded in the same elastic matrix. The normalization factor also renders the calculated D_i^2 insensitive on the cutoff utilized for the nearest neighbors. $\Delta\gamma$ was chosen as 0.1% in the following analysis if not specified. This value is relatively large enough to suppress severe fluctuation in the calculated correlation, and also small enough to give a good resolution for its strain dependence.

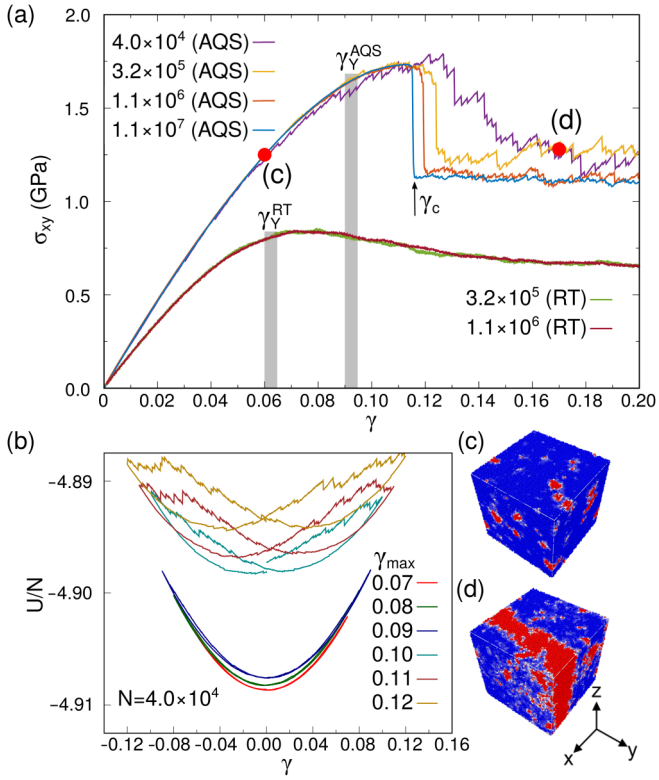

FIG. 1. (a) Stress-strain curves of $Cu_{50}Zr_{50}$ MGs with different system sizes both at AQS and RT. Vertical shadowed areas mark the yielding points ($\gamma_Y = 0.09$ at AQS, and 0.06 at RT). (b) Potential energy vs strain in the steady states of oscillating shear, displaying a bifurcation at the yielding transition between $\gamma_{max} = 0.09$ and 0.1 (with γ_{max} the amplitude of oscillatory shear). Clearly localized plastic zones were observed in (c), while the shear-banding phenomenon was observed in (d), at the strains marked as the red circles on the curve at (a).

III. RESULTS AND DISCUSSION

A. Yielding of metallic glasses

Under an external force, metallic glasses linearly respond to strain at the initial stage, yield at some critical point γ_Y, and finally begin to flow at large strain [Fig. 1(a)]. As the yielding point is the point at which the material starts to plastically deform, a clear-cut definition of it is proposed to be the strain where the sample displays a significant hysteresis in stress or potential energy under oscillatory shear [33]. In the steady state, which is referred to as either the limited configurations that the system periodically visits (in the case of small oscillatory amplitudes) or the plastic-flow regime (in the case of large amplitudes above the yield strain) [34,35], we found that the evolution of potential energy is reversible at the oscillation with strain amplitude $\gamma_{max} < 0.09$, while it bifurcates into two minimums at $\gamma_{max} \geqslant 0.1$ [Fig. 1(b)]. Thus, $\gamma_Y \approx 0.09$ for AQS, consistent with our previous results [28]. Similarly, we found $\gamma_Y \approx 0.06$ for RT alloys with oscillatory shear, clearly

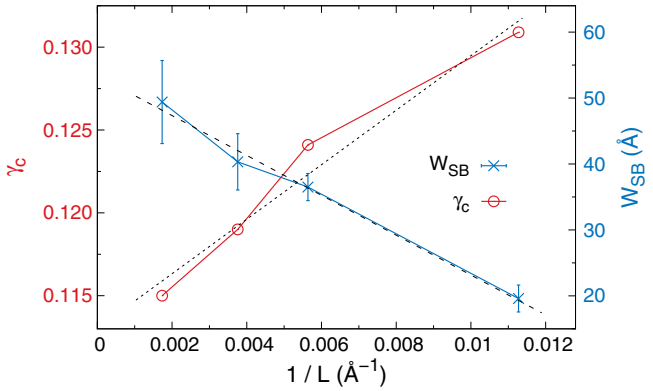

FIG. 2. Critical strain for shear band formation and width of shear bands in AQS alloys. The dotted and dashed lines are the fitting according to Eqs. (2) and (3), respectively.

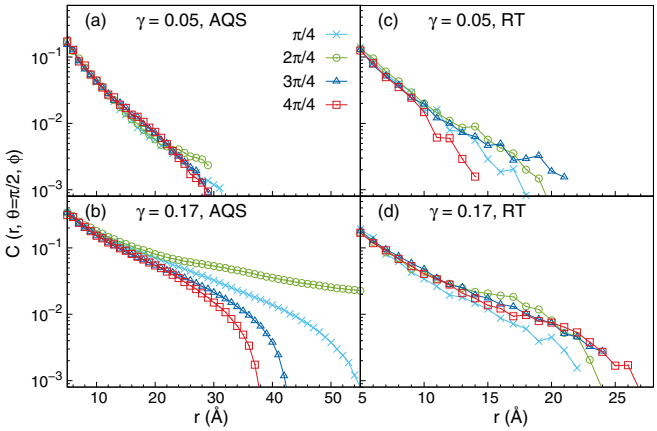

FIG. 3. Nonaffine correlations on the shear plane (x-y plane, $\theta = \pi/2$) along directions: $\phi = \pi/4, \pi/2, 3\pi/4$, and π, with $N = 3.2 \times 10^5$. (a),(b) The correlation in athermal alloys; (c),(d) the correlation in thermal alloys. Top planes are in the elastic regime ($\gamma = 0.05$), with bottom planes in the plastic regime ($\gamma = 0.17$).

less than the reported value ($\gamma_Y \approx 0.1$) in the simulated CuZr MGs at RT with the same embedded-atom method (EAM) potential utilized [18]. The inconsistency comes from the definition discrepancy of the yielding point, which is defined as the maximum position in the stress-strain curve in Ref. [18]. The maximum, however, is dominated by the drastic drop in the stress-strain curve that is due to the shear banding and strongly depends on system size in simulations (which will be discussed later).

In comparison, the stress-strain curve of the RT alloys displays lower yielding stress, weaker overshoot, and the absence of drastic stress drop [Fig. 1(a)]. Thus, the thermal alloys are more ductile, referring to the brittle-to-ductile transition induced by temperature [36]. Additionally, we observe the collapse of the stress-strain curves for different system sizes at RT, viz., no finite-size effect. This gives a hint that the plastic events may not be system spanning in the RT alloys.

Besides the discrepant mechanical properties between thermal and athermal alloys, the microscopic distribution of plastic events also differs; regions of large plastic deformation in the athermal alloys are more heterogeneously distributed and organize into a permanent shear band (SB) at large strain [Figs. 1(c) and 1(d)]. Concomitant with shear banding, stress shows a sudden drop [Fig. 1(a)], which renders an accurate determination of the critical strain (γ_c) for SB emergence in AQS alloys. Intriguingly, the stress drop is more drastic in large systems, indicating a more violent transition to the macroscopic shear localization, in analogy with the percolation phenomenon [37]. We found the associated γ_c for SB formation strongly depends on the system size, in a linear relationship with the inverse of box length L,

$$\gamma_c(L) = \gamma_c(\infty) + B/L, \tag{2}$$

with $\gamma_c(\infty)$ the critical strain in the infinite-size system. The fit (the dotted line in Fig. 2) gives $\gamma_c(\infty) = 0.11$, higher than γ_Y.

A similar finite-size effect was found for the width of SB, W_{SB}, in AQS (see Sec. III C for details of the width calculation),

$$W_{SB}(L) = W_{SB}(\infty) + C/L, \tag{3}$$

with $W_{SB}(\infty)$ the SB width in an infinite-size system. The fit (the dashed line in Fig. 2) gives $W_{SB}(\infty) = 53$ Å, or $19\,R_0$ (with R_0 the diameter of the average atom size). This value is comparable to the simulation of the Lennard-Jones model under oscillatory shear [38], as well as the measured SB thickness in experiments [39,40]. There is a lower limit for the SB width. If L is comparable to the lower limit value, deformation of the sample will become homogeneous, with no shear banding observed (or one may consider that the whole simulation system is inside the SB). It has been reported that there is no SB in a 5000 particle system, while there is in a 40 000 particle system under the oscillatory shear [28].

B. Anisotropic correlation functions

The organization of the plastic events can be characterized by the spatial correlation function, which is generally defined as [41]

$$C(r) = \frac{\langle (A_i - \bar{A})(A_j - \bar{A})\delta[r - |r_{ij}|]\rangle}{\langle (A_i - \bar{A})^2 \delta[r - |r_{ij}|]\rangle}, \tag{4}$$

where A_i is any quantity of atomic attribute, representing $D_i^2(\gamma)$ here. $\langle\cdot\rangle$ denotes the spatial average, and $\bar{A} = \langle A_i\rangle$. It should be noted that $C(r)$ is isotropic. To characterize the anisotropy of plastic correlation, we calculate the azimuthal-dependent correlator $C(r, \theta, \phi)$, where θ is the angle between $\vec{r}$ and the z axis; ϕ is the angle between the projected $\vec{r}$ in the x-y plane with the x axis. As illustrated in Fig. 1(d), we always choose the normal direction of the SB planes as the x axis in athermal alloys.

In the elastic regime for AQS alloys [Fig. 3(a)], decay of the correlators along different directions in the shear plane ($\theta = \pi/2$) collapses together, viz., is isotropic. By contrast, the decay speed strongly depends on the direction in the plastic regime [Fig. 3(b)]. At directions perpendicular to the shear-banding plane ($\phi = 0$ or π), the decay is fast; it gradually slows down on approaching the direction inside the shear band plane ($\phi = \pi/2$). The slow decay at $\phi = \pi/2$ indicates strong correlation between plastic events, and thus an unstable

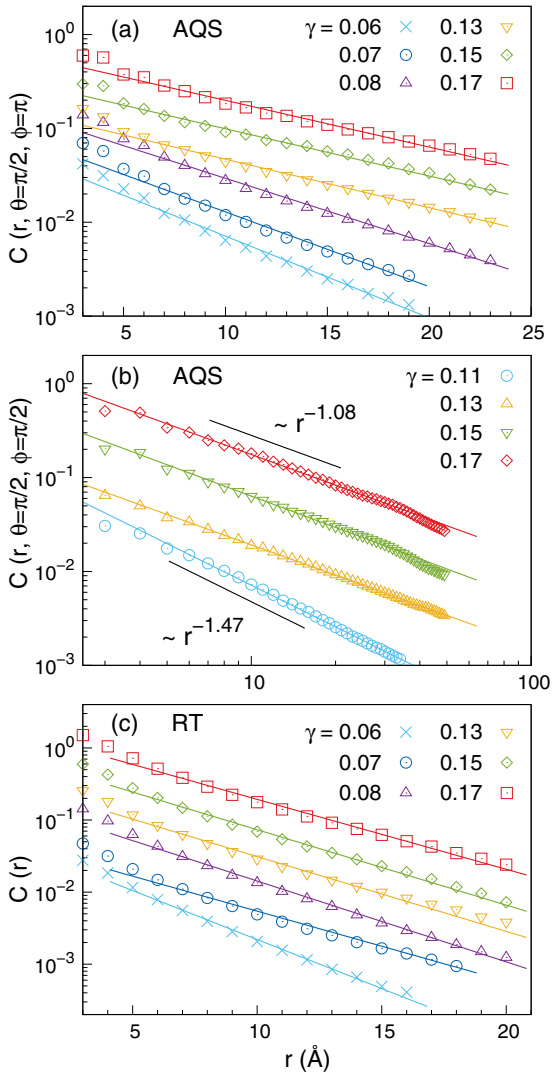

FIG. 4. (a) Nonaffine correlations for athermal alloys at direction perpendicular to the shear-banding plane, and (b) parallel to the shear-banding plane; (c) isotropic correlations for thermal alloys under different shear strains. Solid lines correspond to the fitting via the (a),(c) exponential or (b) power-law formula. Systems are with $N = 3.2 \times 10^5$. Curves are vertically shifted for clarity.

mechanical behavior in this direction. Note that the correlation anisotropy also emerges at the presence of a transient shear band before yielding, as unveiled in soft glassy materials [42].

The anisotropy cannot be observed in thermal alloys. The correlation function nearly collapses together at different directions both in elastic and plastic regimes [Figs. 3(c) and 3(d)], consistent with the reported isotropic correlation in a thermally dominated regime [24].

For athermal alloys, we separate the correlation in different directions. The correlator shows exponential decay in the direction perpendicular to the shear-banding plane [$\phi = \pi$, Fig. 4(a)]. Interestingly, the exponential scaling even holds on at $\gamma > \gamma_c$, with a characteristic length of finite value capturing the correlation in this direction. This may connect with the finite width of the shear band formed in amorphous solids for plastic flow. A power-law decay in the direction parallel to the shear-banding plane was found, i.e., $C(r, \theta = \pi/2, \phi = \pi/2) \propto r^{\beta}$ [Fig. 4(b)]. The algebraic decay reflects the spatial organization principle of plastic events inside the shear band. It should be noted that the power-law decay occurs as early as $\gamma = 0.11$ ($< \gamma_c$), indicating that the strong spatial correlation already exists even before SB formation. The exponent β is about -1.08 at $\gamma > \gamma_c$, coinciding with the theoretical prediction of the nonaffine correlation (where $\beta = 2 - d$, with d the dimensionality) in random elastic media [43]. This suggests that the organization feature of plastic events inside a shear band would be due to the randomness in local moduli coming from the disordered structure.

As the correlation is isotropic in thermal alloys, we azimuthally averaged the correlator, finding it displays an exponential decay both in elastic and plastic regimes [Fig. 4(c)]. The correlator shows fast decay at short distance ($r < 6$ Å). The fast-decay regime has been found to correlate with the neighbor cutoff used for the D_i^2 calculation [18]. The exponential law dictates that the plastic events are not long-range correlated, but localized in a zone with the linear size measurable by a characteristic length. This corresponds to a well-defined shear-transformation zone reported in [15–18]. We fitted the curves via the exponential function, i.e., $C(r) \propto \exp[-r/\xi_{\rm corr}]$, in these cases [see solid lines in Figs. 4(a) and 4(c)], with the obtained characteristic length scale $\xi_{\rm corr}$, summarized in Fig. 7.

C. Spherical harmonic projection

We demonstrate the azimuthal-dependent correlation at different radial distances and strains in Fig. 5. It shows that the correlation is azimuthally homogeneous for AQS alloys in the elastic regime, as well as for RT alloys both in elastic and plastic regimes, coinciding with regimes where the exponential law was found in Fig. 4. At $\gamma > \gamma_c$, regions of positive correlation organize into a narrow band due to the SB formation in athermal alloys (see red-colored regions at $\gamma = 0.17$). Comparing patterns in Figs. 5(a) and 5(b), the width of the positive regions shrinks with r increasing, as the correlator counts more atoms in the elastic matrix that gives a negative value at larger r. Thus, the pattern will be fully colored positive (or red) at small enough r, while it splits into two separate regions if r is larger than the shear-band width. By this, we accurately determined the shear-band width (with the results shown in Fig. 2).

To quantify the azimuthal symmetry of the plastic correlation, we project the correlation function onto the spherical harmonics, $Y_l^m(\theta, \phi)$, analogously to that of the anisotropic pair distribution functions [44–47],

$$C(r, \theta, \phi) = \sum_{l,m} C_l^m(r) Y_l^m(\theta, \phi), \tag{5}$$

where the coefficients, $C_l^m(r)$, are calculated as $C_l^m(r) = \int_0^{2\pi} d\phi \int_0^{\pi} d\theta \sin(\theta) C(r, \theta, \phi) Y_l^{m*}(\theta, \phi)$. Here, Y_l^{m*} is the complex conjugate of the spherical harmonics of degree l and order m. Due to the symmetry, C_l^m is nonzero only if l is even. $l = 0$ presents the isotropic component. The leading terms for the anisotropic components are $l = 2$ for polar symmetry, and $l = 4$ for fourfold (or quadrupolar) symmetry.

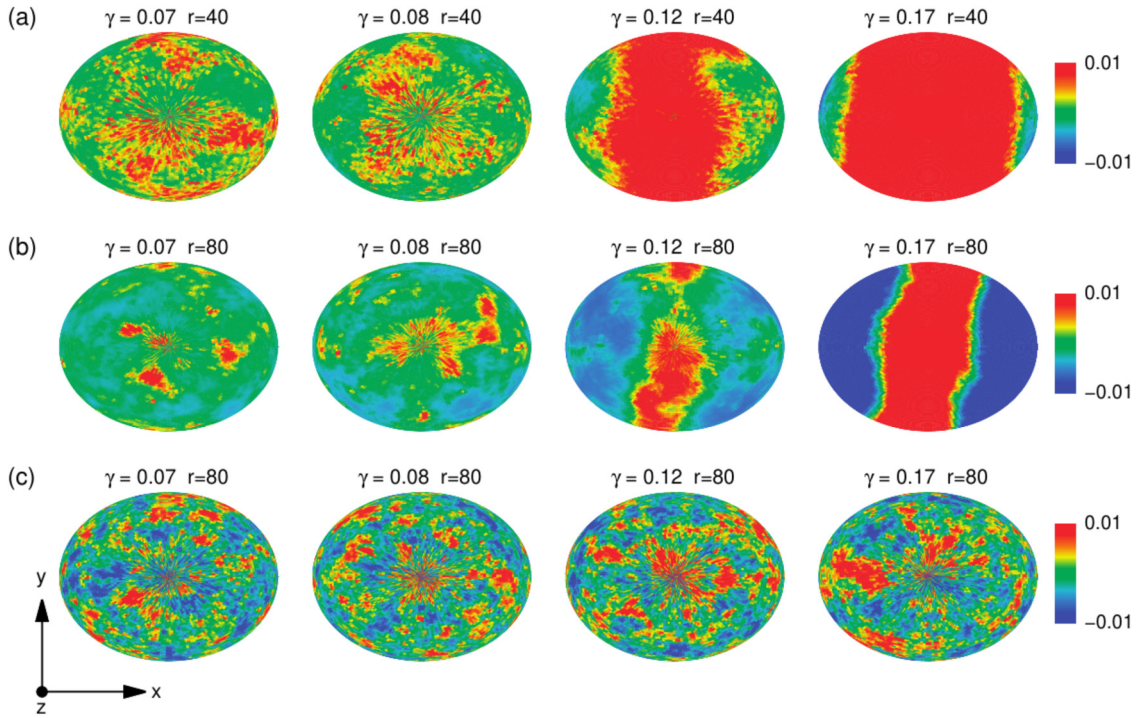

FIG. 5. Azimuthal-dependent correlation function of nonaffine displacement, $C(r, \theta, \phi)$, visualized in Cartesian coordinates at constant r, with (a) $r = 40$ Å for athermal alloys, (b) $r = 80$ Å for athermal alloys, and (c) $r = 80$ Å for RT alloys in the system with $N = 3.2 \times 10^5$. Strain increases from 0.07 to 0.17, from left to right.

We consider the square root of the angular power spectrum: $S_l(r) = [(2l+1)^{-1} \sum_{m=-l}^{l} |C_l^m(r)|^2]^{1/2}$, with the calculated polar and quadrupolar symmetry terms shown in Fig. 6. The spectrum shows a growing tendency with strain in AQS alloys [Figs. 6(a) and 6(b)], and the polar symmetry is the most prominent term when a shear band forms (at $\gamma > \gamma_c$). We also observed the quadrupolar symmetry, with its intensity about one-quarter of the polar component. This fourfold symmetry is not clearly illustrated in Fig. 5 (which will be discussed in Sec. III D). The spectrum displays a nonmonotonic behavior in most of the cases: it increases with r at small distance, while it decreases at longer distance. We define the length scale ξ_{anis} as the position at which the spectrum for $l = 2$ or 4 is maximum. The maximum position shifts to large distance with γ increasing. For thermal alloys without SBs, the spectrum is much weaker [Figs. 6(c) and 6(d)]. It decays rapidly and fluctuates at long distance. In addition, the decay and fluctuation are insensitive to strain. Thus, ξ_{anis} is hard to be analogously defined for these RT alloys, which is consistent with the isotropic behavior observed in the azimuthal-dependent $C(r, \theta, \phi)$ (see Figs. 3 and 5).

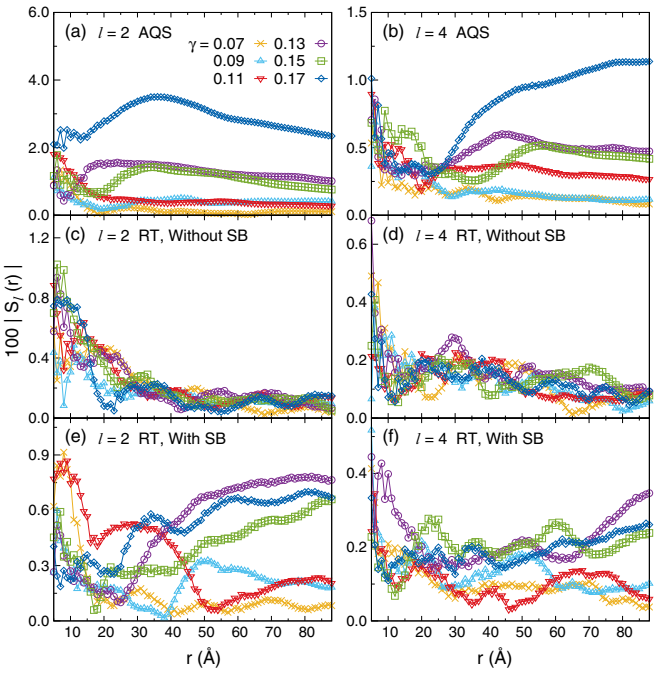

FIG. 6. Angular spectrum of nonaffine displacement correlations in the athermal alloys: (a),(b) the RT alloys without SB, (c),(d) the RT alloys with SB, (e),(f) with $N = 3.2 \times 10^5$. Left panels are for polar symmetry ($l = 2$); right panels are for quadrupolar symmetry ($l = 4$).

D. Discussions

We separate ξ_{anis} from ξ_{corr}; ξ_{anis} mainly measures the distance at which the anisotropy of the correlation reaches the maximum, while ξ_{corr} characterizes the decaying length of the correlation. They are not necessarily similar: ξ_{anis} only considers the azimuthal inhomogeneity regardless of the decaying speed, while it is the opposite for ξ_{corr}.

The obtained ξ_{corr} and ξ_{anis} are summarized in Fig. 7. For AQS alloys, the characteristic length ξ_{corr} monotonically increases with strain, ultimately saturating at γ_c for shear banding [Fig. 7(a)]. As ξ_{corr} was extracted at the direction perpendicular to the SB plane, the saturated value could represent

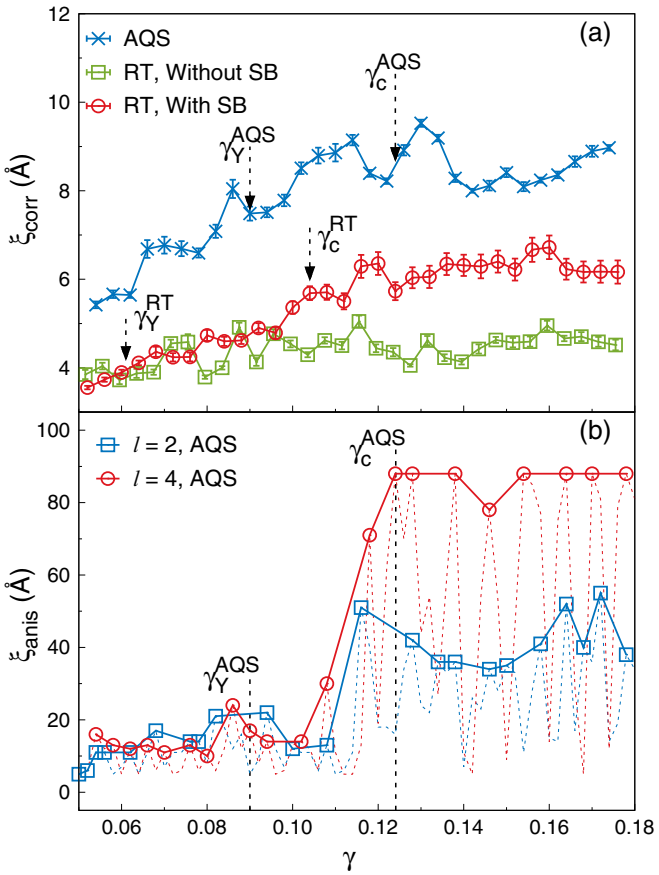

FIG. 7. Characteristic lengths calculated (a) from the correlation of nonaffinity and (b) from the maximum polar ($l = 2$) and quadrupolar ($l = 4$) symmetry in the angular spectrum, with $N = 3.2 \times 10^5$. ξ_{corr} is measured from the isotropic correlation for RT alloys, while is in the direction perpendicular to SB for AQS alloys.

a length scale proportional to the SB width. Surprisingly, we do not observe any significant change at the yielding point γ_Y, at which ξ_{corr} mildly increases; it is also evinced in the case of RT alloys, for which the length shows a fluctuating behavior in the whole strain range [see the sample without SB; open squares in Fig. 7(a)]. This is in contrast to the reported results that a drastic increment of correlation length was observed at the yielding point, and the yielding transition was interpreted as a first-order phase transition [18]. This is due to the fact that the yielding point there is identified as the strain of maximum stress where a SB emerges, as discussed in Sec. III A. The emergence of SB induces an exponential to the power-law decay for the correlation function, as has been illustrated here and also reported in Lennard-Jones systems [48,49]. The transition may lead to a sudden jump in correlations at γ_c if the exponential law is still utilized.

Another discrepancy is that no SB occurs in the RT alloys here compared to Ref. [18], even though the same EAM potential was adopted. A plausible reason is that the samples fabricated here are much less aged, and therefore tend to be more ductile. To check the SB formation, we fabricated more samples using the same protocol, but with different random seeds, finding some to develop a clear SB at γ_c^{RT}. The calculated ξ_{corr} shows a clear increment at small strain, and saturates at γ_c^{RT}, with the tendency similar to that of AQS alloys but the value smaller [open circles in Fig. 7(a)]. The angular spectrum of the harmonic projection in the samples with SBs was shown in Figs. 6(e) and 6(f). The strength of polar symmetry is clearly larger than that without SB at long distance, confirming that the polar symmetry is for the SB emergence. However, it fluctuates with r, without a clear maximum exhibited. The quadrupolar spectrum also fluctuates with r. Thus it is difficult to define the anisotropic length ξ_{anis} in the RT alloys.

Heterogeneous mechanical response in time (or in strain for the AQS protocol) induces a non-negligible fluctuation in the calculated correlations, which can be seen in the widely scattered ξ_{anis} in the plastic regime for AQS alloys [dotted lines in Fig. 7(b)]. The heterogeneity is displayed as the increment of stress interrupted by a sudden drop (the so-called avalanche events) in the stress-strain curve [50,51]. The local nonaffinity exhibits strong correlation when the calculation of nonaffinity covers the stress drop events, while the correlation is weaker when calculated in the strain interval where the stress nearly increases with strain. The anisotropy of the correlation takes this effect into account. ξ_{anis} fluctuates down in the increment interval, while it fluctuates up when the stress drop sets in.

We pick up the maximum positions in the fluctuation corresponding to the time where plastic events burst, finding a drastic increase before γ_c and a saturating behavior after γ_c, both for the correlations of $l = 2$ and $l = 4$ [Fig. 7(b)]. The saturated value for $l = 2$ is around 39 Å, close to the width of SB in this system ($W_{SB} = 37$ Å), verifying that the polar symmetry correlates with the SB formation. The saturated value for $l = 4$ is about 88 Å, the same as the half length of the simulated box, indicating a system-spanning quadrupolar symmetry. This corroborates that the emergence of SB is a percolation phenomenon in amorphous solids, as those reported before [18,48,52]. The system-spanning quadrupolar symmetry only happens at some strains in the flow regime, not at all the strains, due to the mechanical heterogeneity discussed above. Note that the nonaffinity calculated here is instantaneous and an accumulated calculation of it (i.e., setting the reference configuration for D_i^2 calculation always at $\gamma = 0$) will give the results much less affected by the response heterogeneity.

No significant change is found for the correlation lengths (ξ_{corr} or ξ_{anis}) at γ_Y in the simulated RT and AQS alloys, in contrast to the percolation phenomenon observed at yielding in the oscillatory sheared Lennard-Jones solids [33]. This would be ascribed to the deformation protocol that is utilized. In the continuous shear, plastic flow starts at γ_Y, but the flow region can still be localized to some extent and not system spanning before the SB occurrence. Due to the steady state achieved in the oscillatory shear, the localized plasticity percolates the whole system after a number of cycling times, which is evidenced by the fact that an infinite number of cycling times is required at γ_Y to achieve the steady state [35]. Thus, the yielding transition significantly differs here. The plastic events are still, to some extent, localized and homogeneously distributed at strains just beyond γ_Y, verified by the weak signals at the long-distance angular spectrum.

The strain interval for the D_i^2 calculation was set as 0.1% in the correlation functions. This may affect the plastic

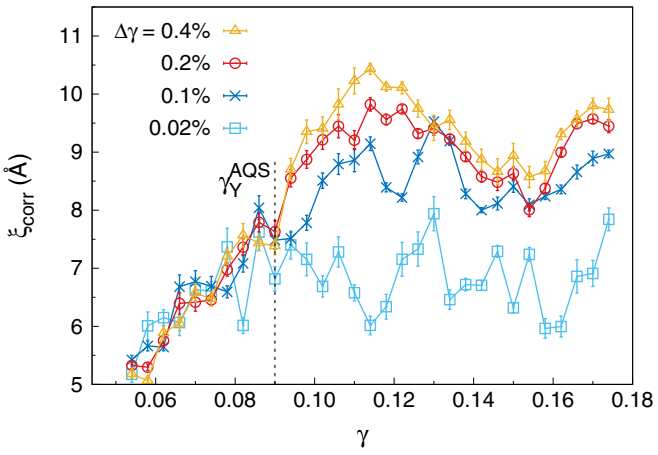

FIG. 8. Correlation lengths obtained for D_i^2 calculated at different strain windows, $\Delta\gamma$, in AQS alloys with $N = 3.2 \times 10^5$.

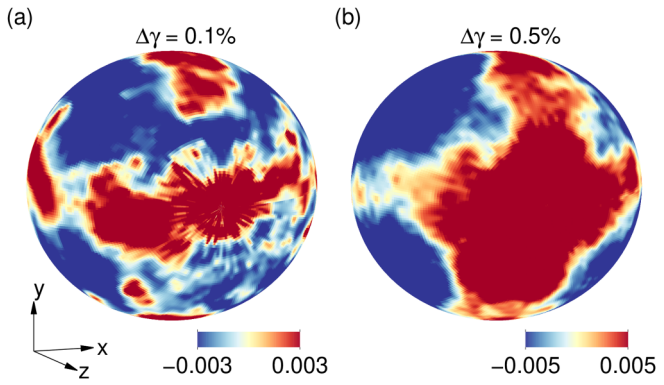

FIG. 9. Azimuthal-dependent correlation function visualized in Cartesian coordinates at $r = 80$ Å for the atoms of large nonaffine displacement (see main text for details). D_i^2 is calculated at (a) $\Delta\gamma = 0.1\%$ and (b) $\Delta\gamma = 0.5\%$, in AQS samples at $\gamma \approx 0.1$ with $N = 3.2 \times 10^5$.

correlation as some plastic events can extend over a larger strain interval, as unveiled by the method of tracing the time-resolved shear transformations [53]. We checked this by varying $\Delta\gamma$ for the D_i^2 calculation. For $\Delta\gamma = 0.02\%$, 0.1%, 0.2%, and 0.4%, we found a similar isotropic-to-anisotropic transition at γ_c in the azimuthal-dependent correlations (results are not shown here). The associated correlation lengths for different $\Delta\gamma$ at the normal direction of SB were shown in Fig. 8. Consistent lengths were obtained for different $\Delta\gamma$ at $\gamma < \gamma_Y$, indicating that the plastic events are spatially localized and occur in a short time or strain window. They deviate from each other at strains beyond γ_Y, implying that the plastic events organize in a longer timescale and are of larger correlation lengths.

We do not observe a clear quadrupolelike symmetry in the nonaffine correlation function as that reported in the steadily sheared 2D amorphous solids [22]. At $\gamma > \gamma_c$, the shear band that is of the polar symmetry dominates the anisotropy of the correlation function, and thus the quadrupolelike symmetry is invisible in this regime. Moreover, before the SB emergence, the quadrupolar field is still absent in the illustrated strains for $C(r, \theta, \phi)$ (see Fig. 5). This could be due to the fact that the correlation was calculated at strains or atoms where the average nonaffine displacement is too small. To this end, we first selected the strain where there is a clear stress drop in the stress-strain curve, e.g., at $\gamma \approx 0.1$ (before shear banding). Second, we calculated $C(r, \theta, \phi)$ for the central atoms of large nonaffine displacement, defined as the atoms whose nonaffinity is larger than some critical value, i.e., $D_i^2 > \bar{D}^2 + 2\sigma$, where $\bar{D}^2$ is the average nonaffinity and σ is its standard deviation. The azimuthal-dependent correlation for D_i^2 calculated at two strain windows is shown in Fig. 9. The quadrupolar symmetry can be clearly seen for D_i^2 calculated with $\Delta\gamma = 0.1\%$, and is more remarkable with $\Delta\gamma = 0.5\%$. Note that the quadrupolar symmetry is only significant at the strains where the stress exhibits a clear drop, even in the case with the selection of the atoms of large nonaffinity. This indicates that the strong correlation between plastic events, which is usually manifested by the burst of avalanche events, is essentially important to detect the quadrupolar symmetry in the nonaffine displacement field.

IV. CONCLUSION

In this work, we performed classical MD simulations on the shear deformation of CuZr metallic glasses at zero and room temperatures. The athermal alloys exhibit higher yielding stress with SBs formed, while the thermal alloys are more ductile. A significant finite-size effect was found for the formation of SBs in the athermal alloys; both the critical strain for the SB emergence and its width linearly scale with the inverse of the simulation box length.

The organization of the plastic events is characterized by the spatial correlation of nonaffine displacement. We found that the correlation function is isotropic and exponentially decays in the alloys without the SB formation. At the presence of SBs, the decay is exponential-like in the SB normal direction, whereas it is power law in the parallel direction. The obtained power-law exponent is about -1, consistent with the theoretical prediction in random elastic media [43]. By projecting the azimuthal-dependent correlations onto the spherical harmonics, we found a strong polar symmetry accounting for the emerged SB, and a weaker quadrupolar symmetry accounting for the displacement field induced by Eshelby inclusions. In the absence of the SB, the quadrupolar field can be clearly visualized in the correlations at the strain where the plastic events burst. We characterized the decaying length ξ_{corr} from the correlators and the anisotropic length ξ_{anis} from the spectrum, finding a saturated length at γ_c, but no significant change at γ_Y. The weak transition in correlation lengths at yielding is ascribed to the localized plastic events, which is also evinced by the isotropic nature of the correlators.

ACKNOWLEDGMENTS

The authors acknowledge financial support from the Natural Science Foundation of Hunan Province, China (Grant No. 2021JJ30833). We are also grateful to the computer resources provided by the High Performance Computing Cluster (HPC) of Central South University.

[1] W. H. Wang, C. Dong, and C. H. Shek, Mater. Sci. Eng. R **44**, 45 (2004).
[2] C. A. Schun, T. C. Hufnagel, and U. Ramamurty, Acta Mater. **55**, 4067 (2007).
[3] B. A. Sun and W. H. Wang, Prog. Mater. Sci. **74**, 211 (2015).
[4] A. Tanguy, J. P. Wittmer, F. Leonforte, and J.-L. Barrat, Phys. Rev. B **66**, 174205 (2002).
[5] C. Goldenberg, A. Tanguy, and J.-L. Barrat, Europhys. Lett. **80**, 16003 (2007).
[6] F. Léonforte, A. Tanguy, J. P. Wittmer, and J.-L. Barrat, Phys. Rev. Lett. **97**, 055501 (2006).
[7] D. J. Lacks and M. J. Osborne, Phys. Rev. Lett. **93**, 255501 (2004).
[8] J. D. Eshelby, Proc. R. Soc. London **241**, 376 (1957).
[9] A. Lemaître and C. Caroli, Phys. Rev. Lett. **103**, 065501 (2009).
[10] V. Chikkadi, G. Wegdam, D. Bonn, B. Nienhuis, and P. Schall, Phys. Rev. Lett. **107**, 198303 (2011).
[11] Y. Wang, Y. Wang, and J. Zhang, Nat. Commun. **11**, 4349 (2020).
[12] A. Lemaître, Phys. Rev. Lett. **113**, 245702 (2014).
[13] S. Chowdhury, S. Abraham, T. Hudson, and P. Harrowell, J. Chem. Phys. **144**, 124508 (2016).
[14] M. Maier, A. Zippelius, and M. Fuchs, Phys. Rev. Lett. **119**, 265701 (2017).
[15] P. Murali, Y. W. Zhang, and H. J. Gao, Appl. Phys. Lett. **100**, 201901 (2012).
[16] E. D. Cubuk, R. J. S. Ivancic, S. S. Schoenholz, D. J. Strickland, A. Basu, Z. S. Davidson, J. Fontaine, J. L. Hor, Y.-R. Huang, Y. Jiang, N. C. Keim, K. D. Koshigan, J. A. Lefever, T. Liu, X.-G. Ma, D. J. Magagnosc, E. Morrow, C. P. Ortiz, J. M. Rieser, A. Shavit *et al.*, Science **358**, 1033 (2017).
[17] D. Wei, J. Yang, M.-Q. Jiang, B.-C. Wei, Y.-J. Wang, and L.-H. Dai, Phys. Rev. B **99**, 014115 (2019).
[18] R. Jana and L. Pastewka, J. Phys. Mater. **2**, 045006 (2019).
[19] S. Mandal, V. Chikkadi, B. Nienhuis, D. Raabe, P. Schall, and F. Varnik, Phys. Rev. E **88**, 022129 (2013).
[20] V. Chikkadi and P. Schall, Phys. Rev. E **85**, 031402 (2012).
[21] F. Varnik, S. Mandal, V. Chikkadi, D. Denisov, P. Olsson, D. Vågberg, D. Raabe, and P. Schall, Phys. Rev. E **89**, 040301(R) (2014).
[22] A. Nicolas, J. Rottler, and J.-L. Barrat, Eur. Phys. J. E **37**, 50 (2014).
[23] F. Puosi, J. Rottler, and J.-L. Barrat, Phys. Rev. E **94**, 032604 (2016).
[24] V. Chikkadi, S. Mandal, B. Nienhuis, D. Raabe, F. Varnik, and P. Schall, Europhys. Lett. **100**, 56001 (2012).
[25] C. Maloney and A. Lemaitre, Phys. Rev. Lett. **93**, 016001 (2004).
[26] M. I. Mendelev, D. K. Rehbein, R. T. Ott, M. J. Kramer, and D. J. Sordelet, J. Appl. Phys. **102**, 093518 (2007).
[27] M. I. Mendelev, M. J. Kramer, R. T. Ott, D. J. Sordelet, D. Yagodin, and P. Popel, Philos. Mag. **89**, 967 (2009).
[28] H. Li, H. Liu, and H. Peng, J. Non-Cryst. Solids **539**, 120069 (2020).
[29] C. E. Maloney and A. Lemaitre, Phys. Rev. E **74**, 016118 (2006).
[30] S. Plimpton, J. Comput. Phys. **117**, 1 (1995).
[31] M. L. Falk and J. S. Langer, Phys. Rev. E **57**, 7192 (1998).
[32] H. L. Peng, M. Z. Li, and W. H. Wang, Phys. Rev. Lett. **106**, 135503 (2011).
[33] P. Leishangthem, A. D. S. Parmar, and S. Sastry, Nat. Commun. **8**, 14653 (2017).
[34] I. Regev, T. Lookman, and C. Reichhardt, Phys. Rev. E **88**, 062401 (2013).
[35] D. Fiocco, G. Foffi, and S. Sastry, Phys. Rev. E **88**, 020301(R) (2013).
[36] H. B. Yu, X. Shen, Z. Wang, L. Gu, W. H. Wang, and H. Y. Bai, Phys. Rev. Lett. **108**, 015504 (2012).
[37] T. Nakayama and K. Yakubo, *Fractal Concepts in Condensed Matter Physics* (Springer, New York, 2003).
[38] A. D. S. Parmar, S. Kumar, and S. Sastry, Phys. Rev. X **9**, 021018 (2019).
[39] C. Liu, V. Roddatis, P. Kenesei, and R. Maaß, Acta Mater. **140**, 206 (2017).
[40] M. R. Chellali, S. H. Nandam, and H. Hahn, Phys. Rev. Lett. **125**, 205501 (2020).
[41] H. L. Peng and T. Voigtmann, Phys. Rev. E **94**, 042612 (2016).
[42] A. LeBouil, A. Amon, S. McNamara, and J. Crassous, Phys. Rev. Lett. **112**, 246001 (2014).
[43] B. A. DiDonna and T. C. Lubensky, Phys. Rev. E **72**, 066619 (2005).
[44] H. L. Peng, M. Z. Li, and W. H. Wang, Appl. Phys. Lett. **102**, 131908 (2013).
[45] Z. Zhang and W. Kob, Proc. Natl. Acad. Sci. USA **117**, 14032 (2020).
[46] W. Dmowski, T. Iwashita, C.-P. Chuang, J. Almer, and T. Egami, Phys. Rev. Lett. **105**, 205502 (2010).
[47] G.-R. Huang, B. Wu, Y. Wang, and W.-R. Chen, Phys. Rev. E **97**, 012605 (2018).
[48] N. V. Priezjev, Metall. Mater. Trans. A **51**, 3713 (2020).
[49] N. V. Priezjev, Phys. Rev. E **94**, 023004 (2016).
[50] J. Antonaglia, W. J. Wright, X. Gu, R. R. Byer, T. C. Hufnagel, M. LeBlanc, J. T. Uhl, and K. A. Dahmen, Phys. Rev. Lett. **112**, 155501 (2014).
[51] N. P. Bailey, J. Schiøtz, A. Lemaitre, and K. W. Jacobsen, Phys. Rev. Lett. **98**, 095501 (2007).
[52] G. P. Shrivastav, P. Chaudhuri, and J. Horbach, Phys. Rev. E **94**, 042605 (2016).
[53] T. Albaret, F. Boioli, and D. Rodney, Phys. Rev. E **102**, 053003 (2020).